Effect of Magnetic Hysteresis on Rotational Losses in Heteropolar Magnetic Bearings

David C. Meeker, *Member, IEEE*, Alexei V. Filatov, *Associate Member, IEEE*, and Eric H. Maslen, *Member, IEEE*

***Abstract*—This paper extends a method for predicting rotational losses for laminated rotors of heteropolar magnetic bearings by using an eddy-current model to include the effect of magnetic hysteresis in the rotor material. It compares the modeling results to the experimental data that were used earlier to assess the loss model neglecting hysteresis. The correction to the total electromagnetic loss in the rotor due to the hysteresis is significant at rotational speeds below 6000 revolutions per minute (RPM), where the model including hysteresis effects provides much better agreement with existing experimental data.**

***Index Terms*—Eddy currents, magnetic bearings, magnetic hysteresis, rotational loss.**

NOMENCLATURE

$\mathbf{a}_i$	ith unit vector.
$\mathbf{B}$	Magnetic field density, tesla.
$\mathbf{b}_i$	ith harmonic component of $\mathbf{B}$.
$\bar{\mathbf{b}}_i$	Average ith harmonic component of $\mathbf{B}$.
d	Journal lamination thickness, meters.
$\mathbf{H}$	Magnetic field strength, ampere/meter.
$\mathbf{h}_i$	ith harmonic component of $\mathbf{H}$.
$\hat{\mathbf{h}}_i$	Complex conjugate of $\mathbf{h}_i$.
$\mathbf{h}_{i,0}$	ith harmonic component of $\mathbf{H}$, evaluated at insulating boundaries.
n	Harmonic index, nondim integer.
P	Power dissipated, watts.
P_n	nth harmonic contribution to power loss, P.
$P_{n,\mathrm{hyst}}$	nth harmonic contribution to power loss due to hysteresis.
p	Power density, watts/m^3.
$\bar{p}$	Average power density, watts/m^3.
p_n	nth harmonic contribution to power density, watts/m^3.
$p_{n,\mathrm{hyst}}$	nth harmonic contribution to power density due to hysteresis.
r	Radial position in the journal, meters.
r_i	Inner radius of the journal, meters.
r_o	Outer radius of the journal, meters.
T	Torque, newton-meters.
T_n	nth harmonic component of the torque.
w	Energy density, joules/m^3.
z	Axial position along the journal, meters.
α	Real part of complex inverse skin depth, m^{-1}.
β	Imaginary part of complex inverse skin depth, m^{-1}.
μ	Magnetic permeability, tesla meter/ampere.
μ_0	Magnetic permeability of a vacuum, $4\pi \times 10^{-7}$ T m/A.
μ_h	Complex permeability, models hysteresis.
μ_n	Harmonic complex permeability.
ϕ_μ	Phase angle associated with hysteresis model.
σ	Electrical conductivity of journal laminations, siemens/meter.
θ	Angular position around the journal, radians.
Ω	Magnetic scalar potential, amperes.
Ω_n	nth harmonic of the magnetic scalar potential.
ω	Rotational rate of journal, rad/s.

I. INTRODUCTION

AN IMPORTANT advantage of magnetic bearings is their potential for reduced rotational losses relative to rolling element and fluid film bearings. To realize this potential, it is important to have a reasonably accurate method of predicting the rotating losses, both to quantify the improvement in design studies and to account for the loss in the final design. In the absence of a mechanical contact, the two primary sources of rotational loss in magnetic bearings are windage and electromagnetic losses. The latter include resistive power losses caused by eddy currents and hysteresis losses. To reduce electromagnetic losses, the rotors of magnetic bearings are typically laminated. This paper deals with modeling both electromagnetic loss mechanisms in laminated rotors of a heteropolar radial bearings, whose magnetic flux paths are predominantly two-dimensional (2-D) (planar).

Interest in losses induced by rotation of the journal through a nonuniform magnetic field has been strong since magnetic bearings became commercially significant. Experimental measurement of the drag torque (here, primarily due to magnetic hysteresis) was reported in 1979 [1]. A study in 1983 [2] established the first strong analytic model for losses due to eddy currents. A method of analyzing eddy-current effects on the attractive force and counter torque was formulated in 1983 [2]. The method assumed a solid rotor (producing impractically high rotational losses) and neglected the hysteresis effects. In 1992 [3], the relative effect of pole sequencing was studied, revealing relatively little effect and suggesting that the prior assumption that a NSSNNSS... orientation was important to minimizing rotating losses was incorrect. A similar experimental study in 1996 [4]

Manuscript received December 6, 2002; revised April 26, 2004. This work was supported by ABB Corporate Research, Ltd.

D. C. Meeker is with Foster-Miller Inc., Waltham, MA 02154 USA (e-mail: dmeeker@ieee.org).

A. V. Filatov is with Calnetix Inc., Cerritos, CA 90703 USA (e-mail: afilatov@calnetix.com).

E. H. Maslen is with the Department of Mechanical and Aerospace Engineering, University of Virginia, Charlottesville, VA 22904 USA (e-mail: ehm7s@virginia.edu).

Digital Object Identifier 10.1109/TMAG.2004.831664

revealed similar results using a rather novel experimental technique. Further experimental results were published in 1998 [5]. A modeling study published in 2002 [6] examined the effect of pole count and pole sequencing, producing analytic relations of potential value in design studies. An important point about the analytic studies of [3], [6] is that they only account for eddy-current effects and do not consider the effects of hysteresis. Examination of the experimental data of [5] reveals a likely effect of hysteresis and, indeed, that study included a very approximate hysteresis effect in modeling the data.

Complementary to the work of Kasarda [5], two of the authors [7] developed a method to predict rotational losses for laminated rotors of heteropolar magnetic bearings using a thin-plate eddy-current model. In that model, the effects of magnetic hysteresis were neglected. It was suggested that hysteresis effects might be included by introducing a complex-valued magnetic permeability. This model assumes that the hysteresis introduces a constant phase lag between $\mathbf{B}$ and $\mathbf{H}$. The model implies an elliptical B–H loop, which only approximately captures the hysteresis phenomenon. A more detailed description of this hysteresis model can be found in [8]. Even though this approximate hysteresis model is rather crude (i.e., ignores saturation and magnetic dynamics effects as well as the difference between the minor and major hysteresis loops), it produces a model which exhibits much better agreement with experimental data at low speeds than the model without any approximation for hysteresis.

II. Hysteresis Model

A very simple model is employed to incorporate the effects of the hysteresis. In this model, described by Stoll [8], the hysteresis introduces a phase difference between sinusoidal $\mathbf{B}$ and $\mathbf{H}$: $\mathbf{B}$ lags $\mathbf{H}$ by an angle ϕ_μ denoted the "hysteresis angle." The harmonics caused by saturation are ignored, and the hysteresis loop becomes an ellipse with the major axis making an angle of $\tan^{-1}\mu$ with the H axis (see Fig. 1). A complex permeability due to hysteresis can be defined through

$$\mathbf{B} = \mu_h \mathbf{H}: \quad \mu_h = \mu e^{-j\phi_\mu}. \tag{1}$$

The dominant models in the simulation of hysteresis phenomena are due to Preisach [9] and Jiles–Atherton [10]. Both models require a time-transient simulation to obtain loss estimates. Such a procedure is very time consuming and produces far more detail than is needed in the steady-state condition explored here.

For steady-state loss situations, a nonlinear complex permeability approach has been explored to estimate hysteresis loss with a greatly reduced computational effort [11]. Generally, good agreement with time-stepping models has been noted, and recent work [11] has focused on deriving a complex-valued B–H curve directly from a Preisach model.

The present work additionally assumes that complex permeability is independent of amplitude. This assumption allows for the inclusion of hysteresis effects while maintaining a description of the eddy currents and hysteresis in terms of linear partial differential equations, greatly simplifying the calculations and allowing for analytical solutions. Because the magnetic bearings are nominally operated at a bias point well below saturation (typically on the order of 0.6–0.8 T), it is reasonable to assume that the material exhibits negligible saturation so that actual hysteresis loops exhibited by the iron are substantially elliptical.

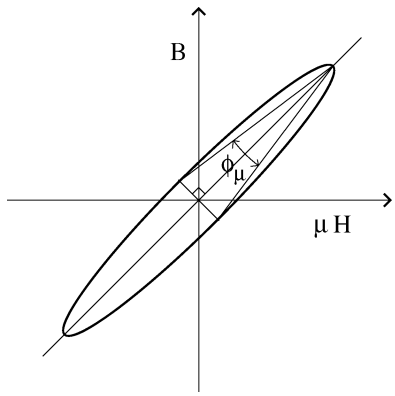

Fig. 1. Approximation of a hysteresis loop.

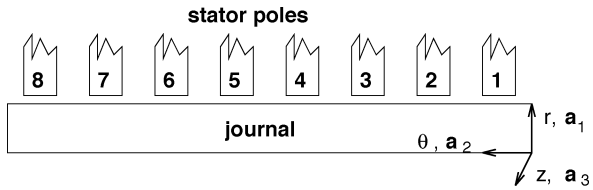

Fig. 2. "Unrolled" heteropolar bearing.

III. Model Development

The development proceeds in a way which is somewhat similar to the development in [7]. To simplify the analysis, it is assumed that the journal of a typical heteropolar magnetic bearing can be "unrolled" into a periodic sheet, as pictured in Fig. 2.

Since the rotor is laminated, a thin-plate model can be assumed in which the r and θ second-order derivative terms in the governing differential equations are so insignificant compared to the z component that they can be neglected altogether. Applying this thin-plate assumption yields a simplified eddy-current model driven by journal motion [7]

$$\frac{\partial^2 \mathbf{H}}{\partial z^2} = \omega \sigma \mu \frac{\partial \mathbf{H}}{\partial \theta} \tag{2}$$

in which ω is the rotational speed of the journal and μ and σ are the permeability and conductivity of the rotor material, respectively.

Since the unrolled domain is 2π periodic in the θ coordinate, the solution for $\mathbf{B}$ is expected to consist of harmonics in θ. A phasor representation can be adopted where $\mathbf{H}$ is defined as [8]

$$\mathbf{H} = \mathrm{Re}\left(\sum_{n=0}^{\infty} \mathbf{h}_n e^{jn\theta}\right) \tag{3}$$

in which $\mathbf{h}_n$ is a complex vector denoting the magnitude and phase of the nth harmonic component of $\mathbf{H}$. Since the system is linear, each harmonic can be considered separately and the results for all harmonics may be superimposed to yield a solution for $\mathbf{H}$.

Substituting the phasor representation for $\mathbf{H}$ into (2) yields

$$\frac{d^2\mathbf{h}_n}{dz^2} = jn\omega\sigma\mu\mathbf{h}_n. \tag{4}$$

In the phasor representation, the field distribution for each harmonic is governed by an ordinary differential equation in z, the coordinate in the plate thickness direction.

With the equations in the form of (4), the complex permeability model of hysteresis can be inserted. The hysteresis model is included simply by replacing permeability μ with complex-valued permeability, μ_h. The differential equation describing the field in the laminations including hysteresis effects is

$$\frac{d^2\mathbf{h}_n}{dz^2} = jn\omega\sigma\mu_h\mathbf{h}_n \tag{5}$$

Equation (5) can be solved subject to the boundary condition $\mathbf{h}_n = \mathbf{h}_{n,o}$ at the insulation between laminations: at both $z = -d/2$ and $z = d/2$. The resulting distribution of $\mathbf{h}_n$ across the lamination is

$$\mathbf{h}_n = \left(\frac{\cosh\left((\alpha+j\beta)z\right)}{\cosh\left((\alpha+j\beta)\frac{d}{2}\right)}\right)\mathbf{h}_{n,o} \tag{6}$$

where d represents the lamination thickness and α and β are defined by

$$\alpha + j\beta \equiv \sqrt{jn\omega\sigma\mu_h}. \tag{7}$$

If $\mathbf{h}_n$ is averaged across the thickness of the lamination and multiplied by μ_h to obtain the average flux density in the lamination, the result can be written as

$$\bar{\mathbf{b}}_n = \mu_n\mathbf{h}_{n,o} \tag{8}$$

where

$$\mu_n = \mu_h\frac{\tanh\left(\sqrt{jn\omega\sigma\mu_h}\frac{d}{2}\right)}{\sqrt{jn\omega\sigma\mu_h}\frac{d}{2}}. \tag{9}$$

For purposes of numerical evaluation and later development in this paper, permeability μ_n can be separated explicitly into real and imaginary parts as

$$\mu_n = \mathrm{Re}(\mu_h)\frac{\alpha\sin(d\beta)+\beta\sinh(d\alpha)}{d\alpha\beta\left(\cos(d\beta)+\cosh(d\alpha)\right)} + j\mathrm{Re}(\mu_h)\frac{\beta\sin(d\beta)-\alpha\sinh(d\alpha)}{d\alpha\beta\left(\cos(d\beta)+\cosh(d\alpha)\right)}. \tag{10}$$

The solution for $\mathbf{H}$ on the face of each lamination must then be related to the solution on the surface of the rotor. Since the axial current density normal is zero at the lamination interface, the 2-D magnetic field distribution in the plane of the lamination interface is curl-free and can be described by a potential function Ω. The field intensity at the lamination interface is defined in terms of the magnetic scalar potential Ω as

$$\mathbf{H}_o = -\nabla\Omega \tag{11}$$

and Ω must obey the partial differential equation

$$\frac{\partial^2\Omega}{\partial r^2} + \frac{1}{r_o^2}\frac{\partial^2\Omega}{\partial\theta^2} = 0 \tag{12}$$

For each individual harmonic

$$\frac{\partial^2\Omega_n}{\partial r^2} - \left(\frac{n}{r_o}\right)^2\Omega_n = 0. \tag{13}$$

Equation (13) can be solved under the boundary condition at the inner radius of the journal

$$\frac{\partial\Omega_n}{\partial r} = 0 \quad \text{at} \quad r = r_i. \tag{14}$$

It can be assumed that the flux in the air gap between the stator inner surface and the rotor outer surface is purely two-dimensional. However, the solution in the lamination is a function of z, as can be seen in (6). To accommodate this discrepancy, it is assumed that a transition between the 2-D solution in the gap and the fully developed profile described by (6) takes place in a very thin skin region near the surface of the rotor. With these assumptions and enforcing the conservation of the flux passing normal to the rotor surface and the continuity of the tangential component of $\mathbf{H}$, it was found in [7] that the magnetic potential describing the field in the air gap is equal to Ω and has to satisfy the following mixed boundary condition on the boundary between the journal iron and the air in the gap:

$$\frac{\partial\Omega_n}{\partial r} = \frac{\mu_n}{\mu_o}\left(\frac{n}{r_o}\right)\tanh\left(\frac{n}{r_o}(r_o - r_i)\right)\Omega_n. \tag{15}$$

The solution for the magnetic field in the bearing can then be found numerically as described in [7], imposing boundary condition (15) on the interface between the air and the rotor, but without having to mesh and solve explicitly within the rotor.

IV. Total Loss Computation

Perhaps the simplest way to derive rotating losses from a field solution is to obtain the torque on the rotor via a stress tensor integration along a closed path through the air encircling the rotor. The computed torque can then be multiplied by the rotational speed to obtain power loss.

The approach taken here is to consider each harmonic of the field at the rotor's surface separately and then sum the results to get the total losses. For the nth harmonic, the amplitude and phase of the field can be represented by the complex-valued vector $\mathbf{h}_n(r_{o+})$. This vector represents the field intensity on the air side of the interface between the air and iron journal (i.e., at $r = r_{o+}$).

The torque associated with each harmonic per lamination can be obtained via Maxwell's stress tensor

$$T_n = (2\pi r_o d)\times r_o \times \frac{\mu_o}{2}\mathrm{Re}\left((\mathbf{h}_n|_{r_{o+}}\cdot\mathbf{a}_1)(\hat{\mathbf{h}}_n|_{r_{o+}}\cdot\mathbf{a}_2)\right) \tag{16}$$

where $\hat{\mathbf{h}}_n$ denotes the complex conjugate of $\mathbf{h}_n$.

The first term in (16) is the surface area of the rotor occupied by one lamination, the second is the moment arm upon which the shear on the rotor is acting, and the third term is the average shear stress on the rotor's surface due to the nth harmonic. Note that no special effort is involved in integrating across the thickness of the lamination, since the field in the air outside the lamination is not a function of z. The amplitude and phase of the field intensity normal to the surface of the rotor is represented

by $(\mathbf{h}_n(r_{o+})\cdot\mathbf{a}_1)$, and that of the tangential magnetic field intensity by $(\mathbf{h}_n(r_{o+})\cdot\mathbf{a}_2)$. The normal portion of the field intensity can be written in terms of the potential by referring to boundary condition (15) at the rotor's surface

$$\begin{aligned}\mathbf{h}_n(r_{o+})\cdot\mathbf{a}_1 &= -\frac{\partial\Omega_n}{\partial r}(r_{o+})\\ &= -\frac{\mu_n}{\mu_o}\left(\frac{n}{r_o}\right)\tanh\left(\frac{n}{r_o}(r_o-r_i)\right)\Omega_n(r_o).\end{aligned}\quad(17)$$

The tangential flux density is obtained via differentiation with respect to θ

$$\mathbf{H}\cdot\mathbf{a}_2 = -\frac{1}{r_o}\frac{\partial\Omega}{\partial\theta}.\quad(18)$$

However, since the phasor transformation has been taken with respect to the θ coordinate, the differentiation with respect to θ is replaced by a multiplication by $j\,n$ for the nth harmonic

$$\mathbf{h}_n(r_{o+})\cdot\mathbf{a}_2 = -j\left(\frac{n}{r_o}\right)\Omega_n(r_o).\quad(19)$$

Inserting (17) and (19) into (16) yields an expression for the torque on one lamination in terms of the potential at the surface of the rotor

$$T_n = -\mathrm{Im}(\mu_n)\pi n^2 d\tanh\left(\frac{n}{r_o}(r_o-r_i)\right)|\Omega_n(r_o)|^2.\quad(20)$$

To obtain the power dissipated in the rotor by the nth harmonic, the torque is simply multiplied by the rotational speed

$$P_n = -\omega\mathrm{Im}(\mu_n)\pi n^2 d\tanh\left(\frac{n}{r_o}(r_o-r_i)\right)|\Omega_n(r_o)|^2.\quad(21)$$

To obtain the total motion-induced power loss, the loss contributions from each harmonic are summed

$$P=\sum_{n=0}^{\infty}P_n.\quad(22)$$

V. Hysteresis Loss

To investigate how much of the loss is due to eddy currents and how much is due to hysteresis, the imaginary part of μ_n can be broken down into a component due to eddy currents and a component due to hysteresis. Since the total loss has already been obtained, it is sufficient to derive just one of the component losses. Here, the hysteresis component will be addressed.

Hollaus and Biro note in [11] that the hysteresis loss density for one cycle is

$$w_{n,\mathrm{hyst}} = -\pi\mathrm{Im}(\mu_h)|\mathbf{h}_n|^2.\quad(23)$$

Since the time required to traverse one complete cycle is $2\pi/(n\omega)$, the time average power loss density due to the hysteresis is

$$p_{n,\mathrm{hyst}} = -\frac{n\omega}{2}\mathrm{Im}(\mu_h)|\mathbf{h}_n|^2.\quad(24)$$

Since $\mathbf{h}_n$ varies across the thickness of the lamination, no general result can be obtained from the point loss expression. However, if the average loss over the thickness of the lamination is computed, the result can be compared to the average total loss across the thickness of the lamination to produce a useful result. The average hysteresis loss density across the thickness of the lamination for the nth harmonic, $\bar{p}$, is obtained via the integral

$$\bar{p}_{n,\mathrm{hyst}} = -\frac{n\omega}{2}\mathrm{Im}(\mu_h)\frac{1}{d}\int_{-\frac{d}{2}}^{\frac{d}{2}}|\mathbf{h}_n|^2dz.\quad(25)$$

To evaluate the hysteresis power integral, the squared magnitude of h_n must be evaluated. The inner product of $\mathbf{h}_n$ from (6) and its complex conjugate yields

$$|\mathbf{h}_n|^2 = \left(\frac{\cos(2\beta z)+\cosh(2\alpha z)}{\cos(d\beta)+\cosh(d\alpha)}\right)|\mathbf{h}_{n,o}|^2.\quad(26)$$

The integral in the expression for hysteresis power loss can then be evaluated

$$\frac{1}{d}\int_{-\frac{d}{2}}^{\frac{d}{2}}|\mathbf{h}_n|^2dz = \frac{\alpha\sin(d\beta)+\beta\sinh(d\alpha)}{d\alpha\beta\left(\cos(d\beta)+\cosh(d\alpha)\right)}|\mathbf{h}_{n,o}|^2.\quad(27)$$

If the result of (27) is compared to the complex expansion of μ_n in (10), the following simplification can be noted:

$$\frac{1}{d}\int_{-\frac{d}{2}}^{\frac{d}{2}}|\mathbf{h}_n|^2dz = \frac{\mathrm{Re}(\mu_n)}{\mathrm{Re}(\mu_h)}|\mathbf{h}_{n,o}|^2\quad(28)$$

so that the average power per unit volume due to hysteresis losses is

$$\begin{aligned}\bar{p}_{n,\mathrm{hyst}} &= -\frac{n\omega}{2}\mathrm{Im}(\mu_h)\frac{\mathrm{Re}(\mu_n)}{\mathrm{Re}(\mu_h)}|\mathbf{h}_{n,o}|^2\\ &= \frac{n\omega}{2}\tan(\phi_\mu)\mathrm{Re}(\mu_n)|\mathbf{h}_{n,o}|^2.\end{aligned}\quad(29)$$

The complex permeability μ_n can be viewed as replacing the lamination with an equivalent purely hysteretic medium with a homogeneous distribution of flux density across the lamination thickness. For this equivalent material, (25) can be applied directly to obtain the average total loss per unit volume (i.e., including both hysteresis and eddy-current effects)

$$\bar{p}_n = -\frac{n\omega}{2}\mathrm{Im}(\mu_n)|\mathbf{h}_{n,o}|^2.\quad(30)$$

The ratio of total losses to hysteresis losses for the nth harmonic can then be obtained by taking the ratio of (29) to (30)

$$\frac{\bar{p}_{n,\mathrm{hyst}}}{\bar{p}_n} = -\tan(\phi_\mu)\frac{\mathrm{Re}(\mu_n)}{\mathrm{Im}(\mu_n)}.\quad(31)$$

VI. Comparison With Experimental Data

The results of modeling with the hysteresis taken into account can now be compared with those obtained without hysteresis [7] and with the experimental data which were used previously to validate the model without hysteresis [5], [7]. The experimental

TABLE I
HIGH-SPEED LOSS RIG DIMENSIONS

parameter	dimension
axial length per bearing	4.4 cm
journal inner radius	2.54 cm
journal outer radius	4.55 cm
number of poles	8
number of turns per pole	94
pole width	1.90 cm
lamination thickness	0.3564 mm
lamination conductivity	$7.46(10^6)$ $(\Omega\ \mathrm{m})^{-1}$
lamination permeability	$3460\mu_o$

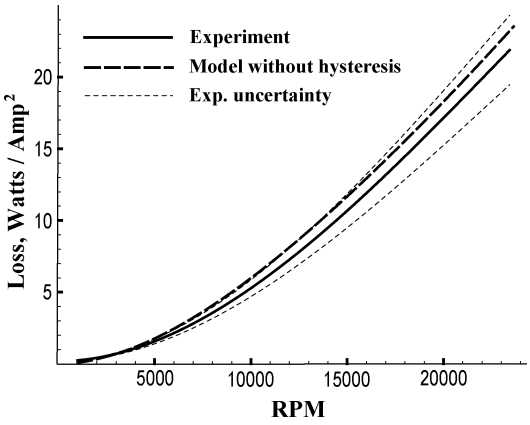

Fig. 3. Experimental and predicted (no-hysteresis) rotational losses in the speed range 1000–24 000 RPM.

measurement of rotational losses was conducted using a test rig (see [5]) which consisted of a short, thick rotor supported by two radial magnetic bearings. There was no thrust bearing; reluctance centering due to the radial bearings was sufficient to keep the rotor centered axially. The rotor was run up to speed using two induction motors located outboard of either bearing. Once the desired maximum speed was obtained, these motors were retracted from the shaft so as not to influence the run-down losses. The relevant dimensions for predicting rotating losses are listed in Table I.

The electromagnetic component of the rotational loss was extracted from the run-down tests using the procedure described in [7] which attempts to distinguish between windage losses and iron losses: the bulk of available data is for tests performed in air at atmospheric pressure. As reported earlier, the results of modeling without hysteresis were in fairly good agreement with the experimental data in the speed range 2500–24 000 revolutions per minute (RPM), as can be seen in Fig. 3 reproduced from [7].

The error envelopes in this figure are due to uncertainty in the measurement of bias current levels for each run-down test. The two boundaries result from calculations based on the nominally specified bias currents and based on the current deduced by the average measured value of flux density in the center of the air gaps. The solid line is the average of these two results. Overall, the predicted losses correspond closely to the measured losses. The model's predictions are within the bounds of experimental uncertainty throughout the range of 2500–24 000 RPM. However, a significant discrepancy is observed at rotational speeds below 2500 RPM (see Fig. 4).

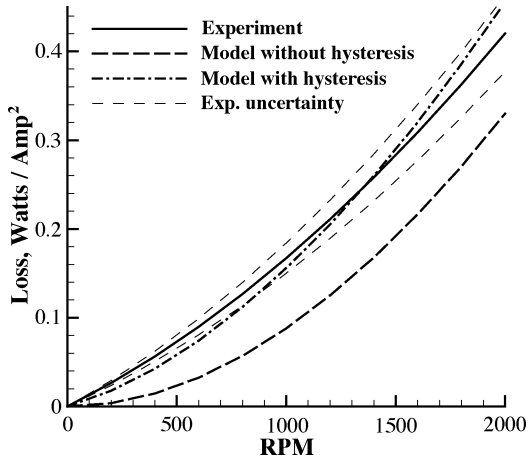

Fig. 4. Experimental and predicted rotational losses in the speed range 0–2500 RPM.

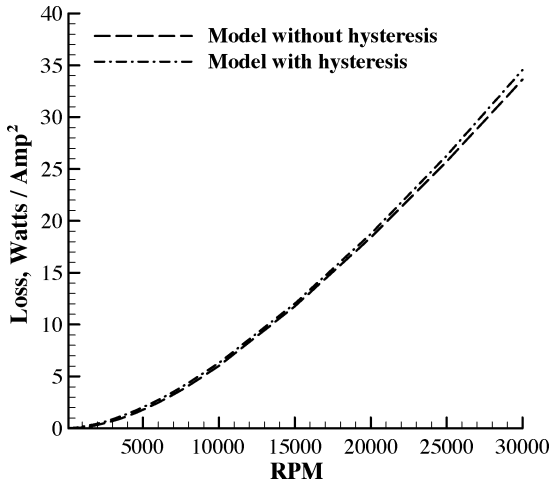

Fig. 5. Comparison of the losses calculated using models with and without hysteresis over speed range 0–30 000 RPM.

If the results of modeling with and without hysteresis are plotted over the whole range of the speeds used in the experiment (0–30 000 RPM), the two graphs can hardly be distinguished (Fig. 5). (The hysteresis angle ϕ_μ was taken to be 20°, as measured in [7]).

However, if this range is limited to 2500 RPM, the difference between the graphs becomes apparent (see Fig. 4). The model including hysteresis effects gives an excellent fit of experimental data at low speeds, while the model ignoring hysteresis significantly underestimates the losses.

The percentage increase of the estimated rotational loss when the hysteresis is taken into account is shown in Fig. 6. The difference between two models is significant (above 10%) if the speed is below 6400 RPM.

At high speeds, the loss calculated with hysteresis is about the same as without hysteresis. However, this does not imply that the proportion of the hysteresis loss component in the total loss is negligible. This can be seen in Fig. 7, which shows that both the calculated total loss and the hysteresis loss increase with rotational speed.

The reason for this is that while the hysteresis effects are causing steadily increasing remagnetization losses, they are also

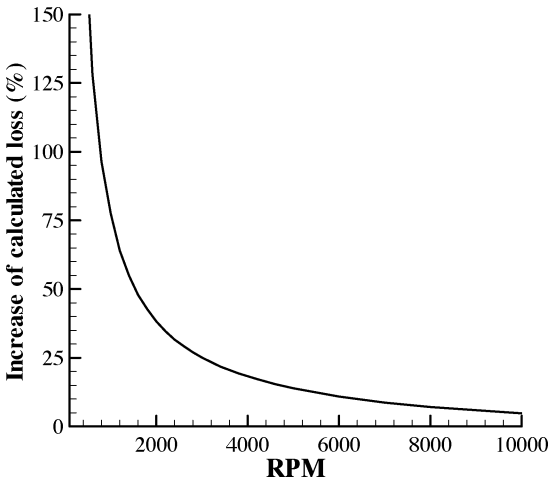

Fig. 6. Calculated loss increase with hysteresis ($\phi_\mu = 20°$).

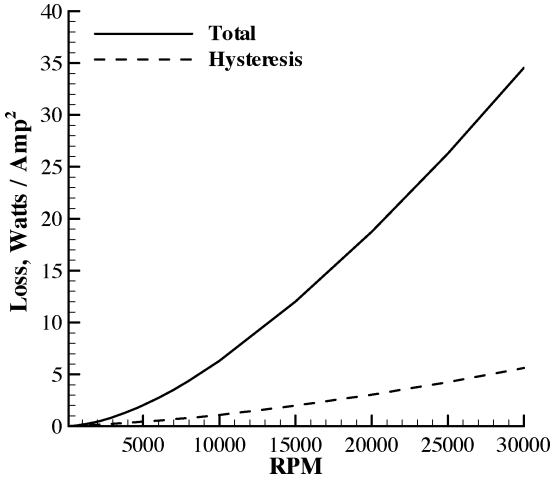

Fig. 7. Calculated total and hysteresis losses.

modifying the magnetic field distribution so that the resistive losses are steadily reduced relative to a nonhysteretic model. Consequently, if the rotational losses with hysteresis were to be estimated by simply summing the eddy-current loss and the hysteresis loss, both calculated using a field distribution obtained without hysteresis, the resulting estimate would significantly exceed the actual losses.

VII. Conclusion

Although hysteresis is a nonlinear effect, it can be adequately modeled in the unsaturated operating regime as a simple phase lag for steady field oscillations. This model permits a linear representation, consistent with the remaining linear analysis of the field including eddy currents. Consequently, it is possible to obtain a tractable, nontransient measure of the combined losses due to eddy currents and hysteresis. The resulting model is consistent with existing experimental data and appears to correct the deficiencies of a nonhysteretic model seen at low speeds while maintaining its fidelity at high speeds. The resulting model is computationally convenient (the solution for an eight-pole stator requires roughly 160 MFLOPS based on a typical solution time of 10 s on an 866-MHz PC). The only additional fitting parameter required in implementing this hysteresis model is the angle ϕ_μ which can be readily obtained from simple impedance testing of a core sample, as described in [7].

The real significance of this predictive capability will depend on the particular application. For systems with relatively high rotation rates, adding hysteresis effects to the analysis will have a negligible effect on the predicted losses: certainly less than the underlying uncertainty of the analysis itself. For systems with relatively low rotation rates, it is important to include hysteresis effects in order to obtain good prediction of losses, but the losses are low enough in this regime that they may be of little practical interest for most applications. However, in low-speed vacuum applications where the only mechanism for heat rejection from the rotor is radiation, these predictions could be crucial to a successful design.

Acknowledgment

The authors would like to express their appreciation for the kind assistance (and data) provided by Dr. M. Kasarda of Virginia Polytechnic Institute.

References

[1] V. S. Vasiliev, A. B. Moma, and G. B. Serdyuk, "Experimental measurement of the drag torque in a magnetic bearing rotor," *Zh. Tekhn. Fiz.*, no. 49, pp. 878–879, Apr. 1979.

[2] T. Yoshimoto, "Eddy current effect in a magnetic bearing model," *IEEE Trans. Magn.*, vol. MAG-19, pp. 2097–2099, Sept. 1983.

[3] F. Matsumura and K. Hatake, "Relation between magnetic pole arrangement and magnetic loss in magnetic bearing," in *Proc. 3rd Int. Symp. Magnetic Bearings*, Alexandria, VA, July 1992, pp. 274–283.

[4] L. S. Stephens and C. R. Knospe, "Effect of magnetic pole arrangement on core loss in laminated high-speed magnetic journal bearings," *IEEE Trans. Magn.*, vol. 32, pp. 3246–3252, July 1996.

[5] M. E. F. Kasarda, P. E. Allaire, E. H. Maslen, G. R. Brown, and G. T. Gillies, "High-speed rotor losses in a radial eight-pole magnetic bearing: Part 1—experimental measurement," *ASME J. Eng. Gas Turbines Power*, vol. 120, pp. 105–109, Jan. 1998.

[6] Y. Sun and L. Yu, "Analytical method for eddy current loss in laminated rotors with magnetic bearings," *IEEE Trans. Magn.*, vol. 38, pp. 1341–1347, Mar. 2002.

[7] D. C. Meeker and E. H. Maslen, "Prediction of rotating losses in heteropolar radial magnetic bearings," *ASME J. Tribol.*, vol. 120, no. 3, pp. 629–635, 1998.

[8] R. L. Stoll, *The Analysis of Eddy Currents*. London, U.K.: Oxford Univ. Press, 1974.

[9] I. D. Mayergoyz, *Mathematical Models of Hysteresis*. New York: Springer-Verlag, 1991.

[10] D. C. Jiles and D. L. Atherton, "Theory of ferromagnetic hysteresis," *J. Magn. Magn. Mater.*, vol. 61, pp. 48–60, 1986.

[11] K. Hollaus and O. Biro, "Derivation of a complex permeability from the Preisach model," *IEEE Trans. Magn.*, vol. 38, pp. 905–908, Mar. 2002.